TRUNCATED LEADING EDGE EFFECTS ON FLOWFIELD STRUCTURE OF A WEDGE IN LOW DENSITY HYPERSONIC FLIGHT SPEED

Wilson F. N. Santos
Instituto Nacional de Pesquisas Espaciais
Laboratório Associado de Combustão e Propulsão
Caixa Postal 01, Cachoeira Paulista, SP 12630-000
wilson@cptec.inpe.br

Abstract. A numerical study was performed to determine the upstream effects of leading edge thickness on the rarefied hypersonic flow over wedges at zero angle of attack. The simulations were performed by using a Direct Simulation Monte Carlo Method. A method that has demonstrated to yield excellent comparisons with flight- and ground-test data, and that properly accounts for nonequilibrium aspects of the flow that arise near the leading edge and that are especially important at high Mach number. Some significant differences between sharp and blunt leading edges were noted on the flowfield structure and on the aerodynamic surface quantities. It was found that the upstream effects have different influence on velocity, density, pressure and temperature along the stagnation streamline ahead of the leading edges. Interesting features observed in the surface fluxes showed that small leading edge thickness compared to the freestream mean free path still has important effects on high Mach number leading edge flows.

Keywords. DSMC, hypersonic flow, rarefied flow, blunt leading edge, wedge.

1. Introduction

Experimental and theoretical works on hypersonic flow past wedges have been concentrated primarily on the analysis of the flowfield by considering the leading edges as being "aerodynamically-sharp". A critical study providing information on maximum allowable edge thickness for a given flow pattern has not received considerable attention. Such information is important when a comparison is to be made between experimental results in the immediate vicinity of the leading edge and the theoretical results, which generally assume a zero-thickness leading edge.

In practice it is extremely difficult to fabricate a perfect sharp tip. Any manufacturing error results in a significant deviation from the design contour and, therefore, sharp edges are difficult to maintain because they are easily damaged. In addition, for practical hypersonic configurations, leading edges must be blunted for heat transfer, manufacturing, and handling concerns. Because blunt leading edge promotes shock standoff, practical leading edges will have shock detachment, making leading-edge blunting a major concern in the design and prediction of flowfields over hypersonic configurations, such as waveriders (Tincher and Burnett, 1994) that are designed analytically with infinity sharp leading edges for shock wave attachment.

There has been a rather limited investigation of the flowfield associated with wedges under hypersonic flow. Cheng et al. (1961) presented the results of a theoretical and experimental study of leading-edge bluntness and boundary layer displacement effects in hypersonic flow over thin bodies. Their theoretical solution was developed based on a continuum flow model in the strong interaction region. Experimental heat transfer and pressure data obtained with two-dimensional wedge models were presented by Vidal and Bartz (1965). The purpose of their investigation was to test the available theories dealing with wedges in a continuum flow in order to define their limits of validity, and to provide data in the transition regime, i.e., between the conventional continuum flow and the free-molecular flow. Their comparison was restricted to the boundary layer theory and the viscous shock layer theory.

McCroskey et al. (1967) investigated experimentally the hypersonic flow on plates, wedges and cones. Pressure and density profiles adjacent to the bodies as well as the shock wave shapes were presented downstream of the leading edges. The results were restricted to the merged layer region, where the shock layer begins to thicken and merges with the boundary layer. Vidal and Bartz (1969) performed a series of low-density experiments with a flat plate at small and large wedge angles. The purpose of their study was twofold: (1) to investigate the viscous shock-layer regime under the combined effects of boundary-layer displacement and wedge angle for plate at small wedge angles, and (2) to investigate the viscous shock-layer regime under conditions where the boundary-layer displacement effects should be negligible, for plate at large wedge angles. The results included direct measurements of surface pressure, skin friction and heat transfer, which were used to infer the jump conditions at the surface.

Allègre et al. (1969) conducted measurements of surface pressure, drag and lift on flat plates and wedges for different values of incidences and leading edge bluntness in a hypersonic flow. The purpose of their investigation was to study the bluntness effect on boundary layer displacement thickness in the hypersonic interaction regime. In this regime, located far downstream of the leading edge, the flow behaves like an ordinary viscous flow with a Prandtl-type boundary layer near the body surface.

Finally, Klemm and Giddens (1977) obtained a solution for the flowfield on a finite-length sharp wedge immersed in a low-density flow. Their results, obtained by employing the Boltzmann equation with the BGK collision model, illustrated the extent of the upstream influence on the macroscopic properties that include the number density and temperature, and the complex nature of the flow in the wake region.

The flowfield properties upstream of the leading edge of a body are affected by molecules reflected from the edge region. The degree of the effect is in part conditioned by the edge geometry. In this context, the purpose of this paper is to investigate the effect of the leading edge thickness on the flowfield structure and on the aerodynamic surface quantities over truncated wedges.

The upstream disturbances on flowfield properties due to changing in the leading edge thickness will be investigated for a range of Knudsen number, based on the thickness of the leading edge, covering from the transition regime to the free molecular flow. The flow conditions represent those experienced by a spacecraft at an altitude of 70 km. This altitude is associated with the transitional regime, which is characterized by the overall Knudsen number of the order of 10^{-2} or larger. Therefore the focus of the present study is the low-density region in the upper atmosphere, where numerical gaskinetic procedures are available to simulate hypersonic flows. High-speed flows under low-density conditions deviate from a perfect gas behavior because of the excitation of rotation, vibration and dissociation. At high altitudes, and therefore low density, the molecular collision rate is low and the energy exchange occurs under nonequilibrium conditions. In such a circumstance, the degree of molecular nonequilibrium is such that the Navier-Stokes equations are inappropriate. In the current study, a Direct Simulation Monte Carlo (DSMC) method is used to calculate the rarefied hypersonic two-dimensional flow.

2. Computational Method and Procedure

A number of significant problems in fluid mechanics involve transitional flows, i.e., flows for which the mean free path is of the same order of magnitude as a characteristic dimension of the problem. The most successful numerical technique for modeling complex transitional flows has been the Direct Simulation Monte Carlo (DSMC) method (Bird, 1994). DSMC has been recognized as an extremely powerful technique capable of predicting an almost unlimited variety of rarefied flowfields in the regimes where neither the Navier-Stokes nor the free molecular approaches are appropriate.

DSMC models the flow as being a collection of discrete particles, each one with a position, velocity and internal energy. The state of the particles is stored and modified with time as the particles move, collide, and undergo boundary interactions in simulated physical space. The physical space is represented by a computational cell network. The cell provides a convenient reference for the choice of the potential collision pairs and for the sampling of the macroscopic gas properties. The dimensions of the cells must be such that the change in flow properties across each cell is small. The linear dimensions of the cells should be small in comparison with the scale length of the macroscopic flow gradients in the streamwise directions, which means that the cell dimensions should be of the order of the local mean free path or even smaller (Bird, 1994). The smallest unit of physical space is the subcell, where the collision partners are selected for the establishment of the collision rate. In addition, an essential feature of the DSMC method is that the molecular motion and collisions are actually uncoupled over the period of a specific time step, and predictions of the new positions of the molecules as well as the resulting boundary interactions are followed by the selection of a set of possible intermolecular collisions that are appropriate during the time step. In general. the step ought to be sufficiently small in comparison with the local mean collision time (Bird, 1994).

In this study, the molecular collisions are modeled using the variable hard sphere (VHS) molecular model (Bird, 1988). This model employs the simple hard sphere angular scattering law so that all directions are equally possible for post-collision velocity in the center-of-mass frame of reference. However, the collision cross section depends on the relative speed of colliding molecules. The energy exchange between kinetic and internal modes is controlled by the Borgnakke-Larsen statistical model (Borgnakke and Larsen, 1975). The essential feature of this model is that a part of collisions is treated as completely inelastic. Simulations are performed using a nonreacting gas model consisting of two chemical species, N_2 and O_2. Energy exchanges between the translational and internal modes are considered. The vibrational temperature is controlled by the distribution of energy between the translational and rotational modes after an inelastic collision. The probability of an inelastic collision determines the rate at which energy is transferred between the translational and internal modes after an inelastic collision. For a given collision, the probabilities are designated by the inverse of the relaxation numbers, which correspond to the number of collisions necessary, on average, for a molecule to relax. The relaxation numbers are traditionally given as constants, 5 for rotation and 50 for vibration.

The freestream and flow conditions used in the present calculations are those given by Bertin (1994) and summarized in Table 1. The freestream velocity U_∞ is assumed to be constant at 3.5 Km/s, which corresponds to freestream Mach number M_∞ of 12. The wall temperature T_w is assumed constant at 880 K. Also, diffuse reflection with full thermal accommodation is assumed for the gas-surface interactions.

The truncated wedges to be analyzed in this work are modeled by assuming a sharp leading edge of half angle θ with a circular cylinder of radius R inscribed tangent to this sharp leading edge. The truncated wedges are also tangent to the sharp leading edge and the cylinder at the same common point. It was assumed that the leading edge half angle is 10°, a circular cylinder diameter of 10^{-2}m and truncated wedge thickness t/λ_∞ of 0.01, 0.1 and 1.0. Figure 1 illustrates schematically the wedges with the truncated leading edges. L and H are obtained in a straightforward manner.

Table 1: Freestream Conditions and Flow Parameters

Working fluid		N_2+O_2	
Altitude		70	Km
Temperature (T_∞)		220.0	K
Pressure (p_∞)		5.582	N/m^2
Density (ρ_∞)		8.753 x 10^{-5}	Kg/m^3
Number density (n_∞)		1.8209 x 10^{21}	m^{-3}
Viscosity (μ_∞)		1.455 x 10^{-5}	Ns/m^2
Velocity (U_∞)		3.56	Km/s
Mean free path (λ_∞)		9.03 x 10^{-4}	m
Mach number (M_∞)		12	
Molecular weight		28.96	Kg/KgMole
Mole fraction	O_2	0.237	
Mole fraction	N_2	0.763	
Molecular mass	O_2	5.312 x 10^{-26}	Kg
Molecular mass	N_2	4.65 x 10^{-26}	Kg
Molecular diameter	O_2	4.01 x 10^{-10}	m
Molecular diameter	N_2	4.11 x 10^{-10}	m
Degree of freedom	O_2	5	
Degree of freedom	N_2	5	

The overall Knudsen number *Kn* is defined as the ratio of the molecular mean free path λ_∞ in the freestream gas to a characteristic dimension of the flowfield. In the present study, the characteristic dimension was defined as being the thickness *t* of the truncated leading edges. For the thicknesses investigated, t/λ_∞ = 0.01, 0.1 and 1.0, the overall Knudsen numbers correspond to Kn_t = 100, 10 and 1, respectively. The Reynolds number Re_t covers the range from 0.193 to 19.3, based on conditions in the undisturbed stream with leading edge thickness *t* as the characteristic length.
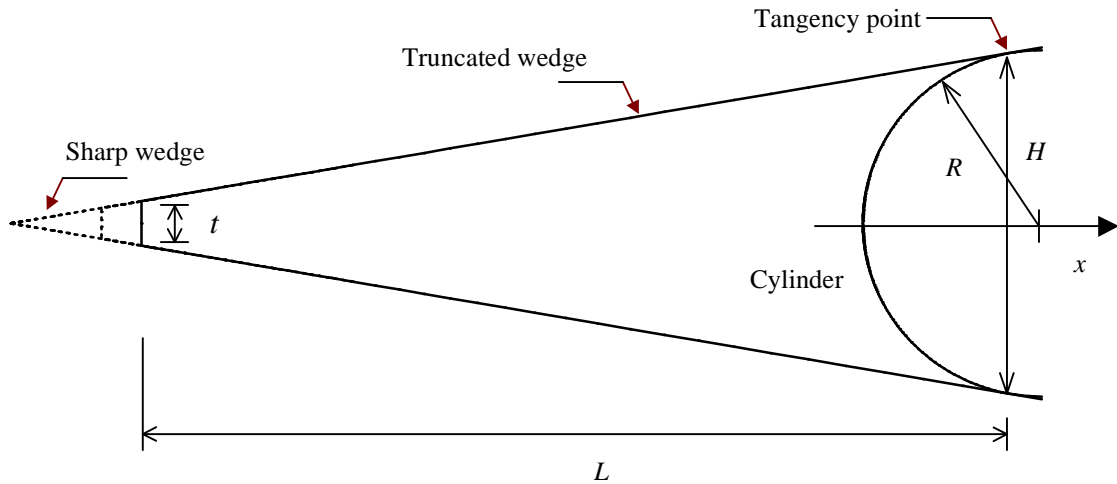

Figure 1: Schematic view of the truncated wedges.

3. Computational Results and Discussion

Attention is now focused on the calculations of the flowfield properties and aerodynamic surface quantities obtained from the DSMC results. Simulations were performed for leading edge thicknesses t/λ_∞ of 0.01, 0.1, 1.0. The present calculations correspond to freestream Mach number of 12, wall temperature of 880 K, and freestream conditions associated to an altitude of 70 Km.

3.1. Flowfield Structure

The flowfield properties of particular interest in the transition flow regime are the normal velocity, density, pressure and temperature. The purpose of this section is to discuss and to compare differences in the profiles of these properties along the stagnation streamline, normalized by the corresponding freestream values, due to variations in the leading edge thickness.

Normal velocity profiles along the stagnation streamline and their dependence on the leading edge thickness are

illustrated in Fig. (2a). Each profile has been taken through cell centroids that lie very close to the stagnation line, and therefore can be considered as being along the stagnation streamline. In Fig. (2a), the normal velocity u is expressed as a fraction of the freestream velocity U_∞, and x/λ_∞ is the dimensionless distance upstream the wedge.

In simulating rarefied flows, the computational flow domain must extent far enough upstream of the body in order to provide ample opportunity for freestream molecules to interact with those molecules that have reflected from the body and are diffusing into the flow. Insufficient upstream domain size leads to overprediction of aerodynamic heating and forces (Haas and Fallavollita, 1994). Figure (2a) demonstrates that the leading edge thickness influences the flowfield far upstream. This domain of influence increases with increasing the leading edge thickness. This results from the upstream diffusion of particles that are reflected from the nose of the leading edge. Therefore, blunting the nose of the wedge (increasing t) leads to significantly larger disturbance upstream of the body. For instance, the upstream distance for a velocity reduction of 1% ($u/U_\infty = 0.99$) is around $1.6\lambda_\infty$, $1.8\lambda_\infty$, $2.4\lambda_\infty$ and $4.5\lambda_\infty$ for cases $t/\lambda_\infty = 0.0$, 0.01, 0.1 and 1.0, respectively.

Figure (2b) displays the velocity slip u_w profiles, normalized by the freestream velocity U_∞, along the body surface as a function of the dimensionless arc length s/λ_∞ measured from the shoulder of the wedge. It is seen that velocity slip presents the maximum value at the shoulder of the leading edges and decreases downstream along the wedge. As the leading edge thickness increases the velocity slip decreases. It means that the outer extent of the flowfield disturbance above the surface is much smaller for the sharp leading edge case than those for blunt leading edge cases. For the $t/\lambda_\infty = 0.0$ case the maximum velocity slip is around 33% of the freestream velocity. On the other hand, for the $t/\lambda_\infty = 1.0$ case, the maximum velocity slip is 15% of the freestream velocity.

It is seen from Figs. (2a) and (2b) that for the truncated wedge with thickness of one hundredth of the freestream mean free path, the normal velocity and the velocity slip are not strongly affected, as compared to the sharp wedge case.
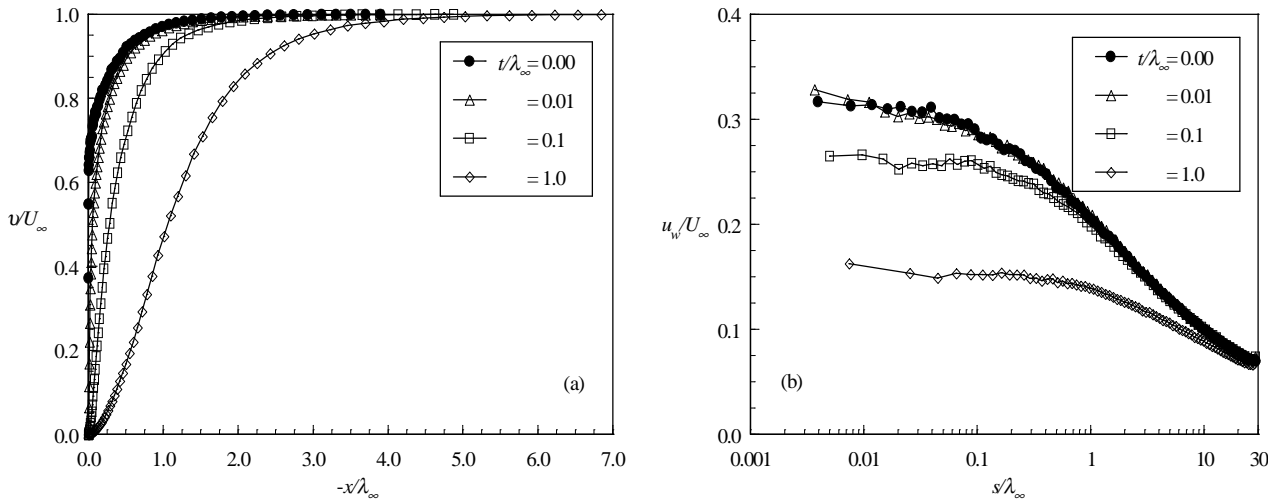

Figure 2: (a) Normal velocity profiles along the stagnation streamline, and (b) velocity slip profiles along the wedge surface as a function of the leading edge thickness.

Density profiles along the stagnation streamline are plotted as a function of the leading edge thickness in Fig. (3a). The predictions of density for all of the leading edge thicknesses investigated show no sign of a discrete shock wave. Instead, there is a continuous rise in density from the freestream to the nose of the wedge, rising to well above the continuum inviscid limit. As a point of reference, the Rankine-Hugoniot relations give a postshock density that corresponds to the ratio $\rho/\rho_\infty = 5.8$ for freestream Mach number of 12. Near the stagnation point ($-x/\lambda_\infty = 0$), a substantial density increase occurs which is a characteristic of cold-wall entry flow (Haas and Fallavollita, 1994). In typical entry flow, the body surface temperature is low compared with the stagnation temperature. This leads to a steep density gradient near the body surface. For the present simulation, the ratio of wall temperature to stagnation temperature is 0.13, which corresponds to a cold-wall flow.

It can be observed from these density profiles that density rises gradually as the flow approaches the nose of the wedge, indicating the diffuse nature of the shock wave, a characteristic of highly rarefied flows. As the leading edge becomes blunter, the extent of the flowfield disturbances becomes much larger, as evidenced by the density profiles. Much of the density increase in the shock layer occurs after the temperature has reached its postshock value, as will be seen later.

For the flow conditions in the present simulation (Table 1), the free molecular flow equations (Bird, 1994) give a density ratio of 9.89, at the stagnation point for the truncated wedges. As can be seen, the density ratio for the $t/\lambda_\infty = 0.01$ case is approaching the free molecular value at the stagnation point.

Figure (3b) illustrates the dimensionless wall density profiles as a function of the dimensionless arc length along the body surface measured from the wedge shoulder. In general, blunting the wedge increases the wall density ratio in the vicinity of the shoulder. Furthermore, it is seen that the wall density rise, resulted from the thickness increase,

diminishes downstream along the wedge surface in a distance of the order of the thickness t.
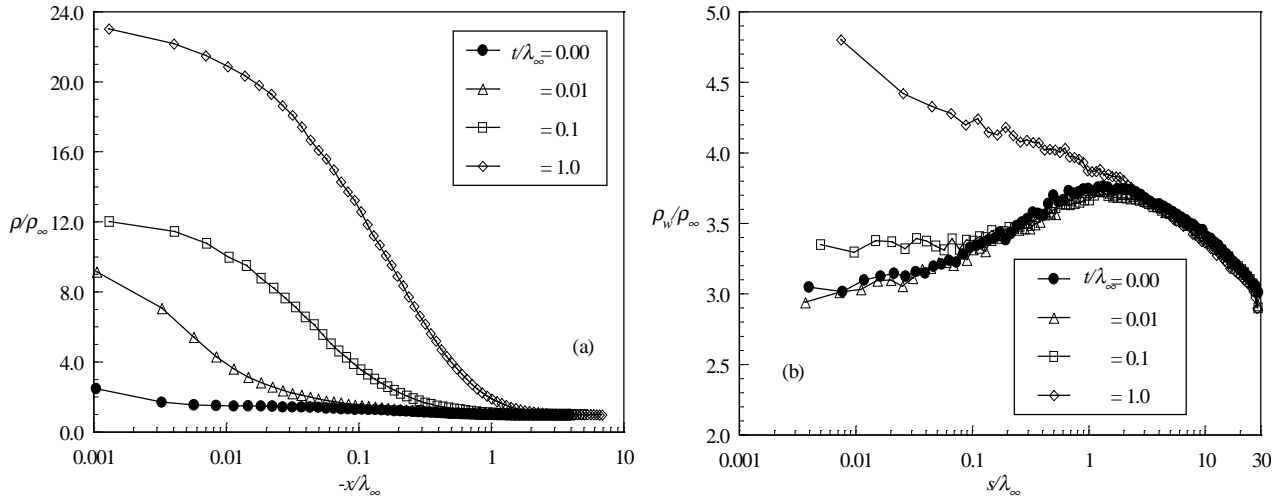
Figure 3: (a) Density profiles along the stagnation streamline, and (b) wall density profiles along the wedge surface as a function of the leading edge thickness.

Figures (4a)-(4d) show the kinetic temperature profiles, normalized by the freestream temperature T_∞, along the stagnation streamline for dimensionless leading edge thicknesses of 0.0, 0.01, 0.1 and 1.0, respectively. From these Figs., thermodynamic nonequilibrium is observed throughout the shock layer, as shown by the lack of equilibrium of the translational and internal kinetic temperatures. Thermal nonequilibrium occurs when the temperatures associated with the translational, rotational, and vibrational modes of a polyatomic gas are different.

The overall kinetic temperature shown is defined for a nonequilibrium gas as the weighted mean of the translational and internal temperature (Bird, 1994). It is important to observe that the ideal gas equation of state does not apply to this temperature in a nonequilibrium situation. The overall kinetic temperature is equivalent to the thermodynamic temperature only under thermal equilibrium conditions.

According to the Figs. (4a)-(4d) in the undisturbed freestream far from the body, the translational and internal temperatures have the same value and are equal to the thermodynamic temperature. Approaching the nose of the leading edge, the translational temperature rises to well above the rotational and vibrational temperatures and reaches a maximum value that is a function of the leading edge thickness. Still further upstream toward the nose of the wedge, the translational temperature decreases (for blunt leading edges) and reaches a value on the wall that is above the wall temperature, resulting in a temperature jump as defined in continuum formulation (Gupta et. al., 1985). The temperature jump decreases as the leading edge thickness increases.

The substantial rise in translational kinetic temperature for the blunt leading edges occurred before the density rise (see Fig. (3a)). For instance, the kinetic translational temperature reaches the maximum value at a distance of one freestream mean free path from the nose of the leading edge for the $t/\lambda_\infty = 1.0$ case, while the density ratio ρ/ρ_∞ is around 1.9 at the same station. The initial translational kinetic temperature rise for blunt leading edges results from the essentially bimodal velocity distribution: the molecular sample consisting of mostly undisturbed freestream molecules with the molecules that have been affected by the shock and reflected from the body. In this way, the translational kinetic temperature rise is a consequence of the large velocity separation between these two classes of molecules. The bimodal velocity distribution was pointed out by Liepmann et al.(1964).

Blunting the leading edge moves the shock wave created during the hypersonic flight forward and out, away from the leading edge, creating an air pocket in front of it. This strong shock wave that forms ahead of a bunt leading edge at hypersonic flow converts the kinetic energy of the freestream air molecules into thermal energy. This thermal energy downstream of the shock wave is partitioned into increase the translational kinetic energy of the air molecules, and into exciting of other molecular energy states such as rotation and vibration (see Figs. (4a)-(4d)). Most of the energy remains with the air molecules as they flow around the body. As a result, the heat flux to the body surface will be relatively low, as shown later.

Pressure profiles along the stagnation streamline are shown in Fig. (5) as a function of the leading edge thickness. In this Fig., pressure is normalized by the freestream pressure p_∞. As can be seen, there is a continuous rise in pressure from the freestream up to the nose of the leading edge. Near the stagnation point, a substantial pressure increase occurs. This pressure increase is a function of the leading edge thickness t. The extent of the upstream flowfield disturbance for pressure is significantly different from those presented by density and temperature. The domain of influence for pressure is higher than that for density and lower than that presented for temperature. Similar to the density, much of the pressure increase in the shock layer occurs after the translational kinetic temperature has reached its postshock value.
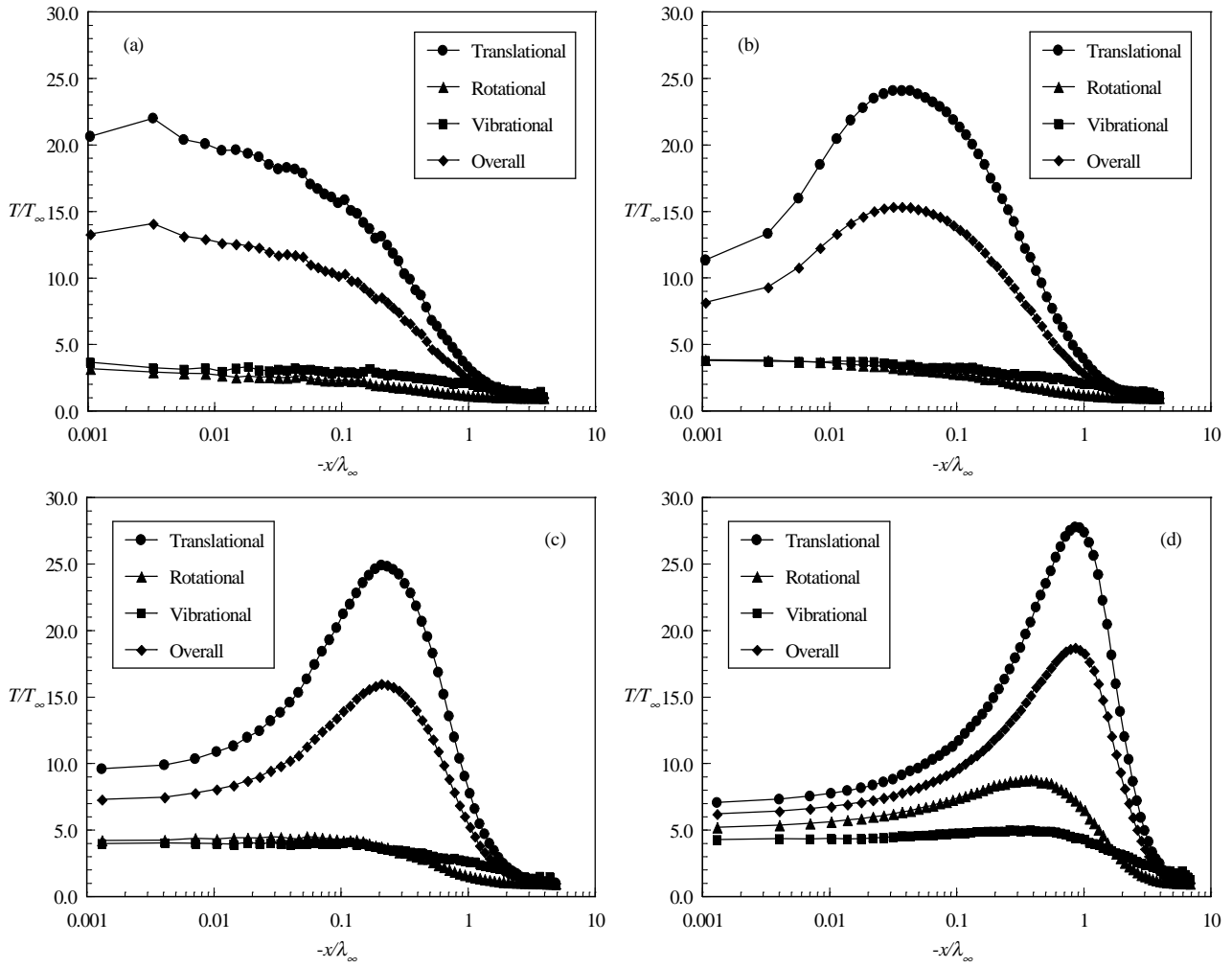
Figure 4: Kinetic temperature profiles along the stagnation streamline for wedges with t/λ_∞ of (a) 0.0, (b) 0.01, (c) 0.1 and (d) 1.0.
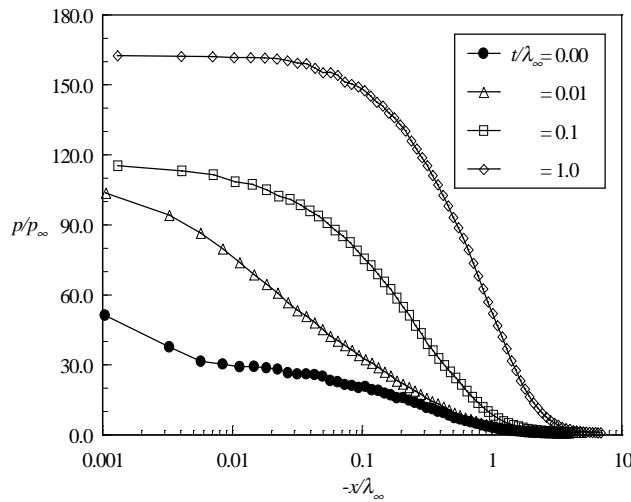

Figure 5: Pressure profiles along the stagnation streamline as a function of the leading edge thickness.

3.2. Surface Quantities

Aerodynamic surface quantities of particular interest in the transition flow regime are number flux, pressure, heat transfer, skin friction and drag. The purpose of this section is to present and to discuss these quantities, expressed in coefficient form, due to variations in the leading edge thickness.

The number flux N is calculated by sampling the molecules impinging on the surface by unit time and unit area.

Results are normalized by $n_\infty U_\infty$, where n_∞ is the freestream number density and U_∞ is the freestream velocity. The sensitivity of the dimensionless number flux to variations on the leading edge thickness is illustrated in Fig. (6). Figure (6a) shows the dimensionless number flux to the frontal face as a function of the dimensionless height y/λ_∞, measured from the stagnation point to the shoulder of the wedge. The dimensionless number flux along the wedge surface is plotted in Fig. (6b) as a function of the dimensionless arc length s/λ_∞, measured from the shoulder of the leading edge. Also, both Figs. present the free molecular flow limit (FM) for the dimensionless number flux by assuming free collision flow (Bird, 1994).

It is seen from Fig. (6a) that the dimensionless number flux is high near the stagnation point and decreases along the frontal face up to the wedge shoulder. As the leading edge thickness decreases the dimensionless number flux to the frontal face decreases and approaches the limit value obtained by the free molecular flow equations (Bird, 1994).

According to Fig. (6b), the dimensionless number flux to the surface also relies on the leading edge thickness. For a sharp wedge ($t/\lambda_\infty = 0.0$), the dimensionless number flux is low at the leading edge and increases substantially up to a maximum value at about $1.0\lambda_\infty$ from the shoulder. A similar behavior is seen for slightly blunt leading edges ($t/\lambda_\infty \leq 0.1$). On the other hand, for the bluntest leading edge case investigated ($t/\lambda_\infty = 1.0$), the dimensionless number flux is large at the shoulder, and decreases gradually along the body surface. One possible reason for this increase in the dimensionless number flux with increasing the leading edge thickness may be related to the collisions of two groups of molecules; the molecules reflecting from the body and the molecules oncoming from the freestream. The molecules that are reflected from the body surface, which have a lower kinetic energy interact with the oncoming freestream molecules, which have a higher kinetic energy. Thus, the surface-reflected molecules recollide with the body surface, which produce an increase in the dimensionless number flux in this region.

Referring to Fig. (6b), it is seen that the downstream influence of the leading edge thickness on the dimensionless number flux is approximately the order of the thickness t. By comparing to the free molecular limit, the dimensionless number fluxes to the inclined surface of the wedges are well above the value predicted by free molecular flow.
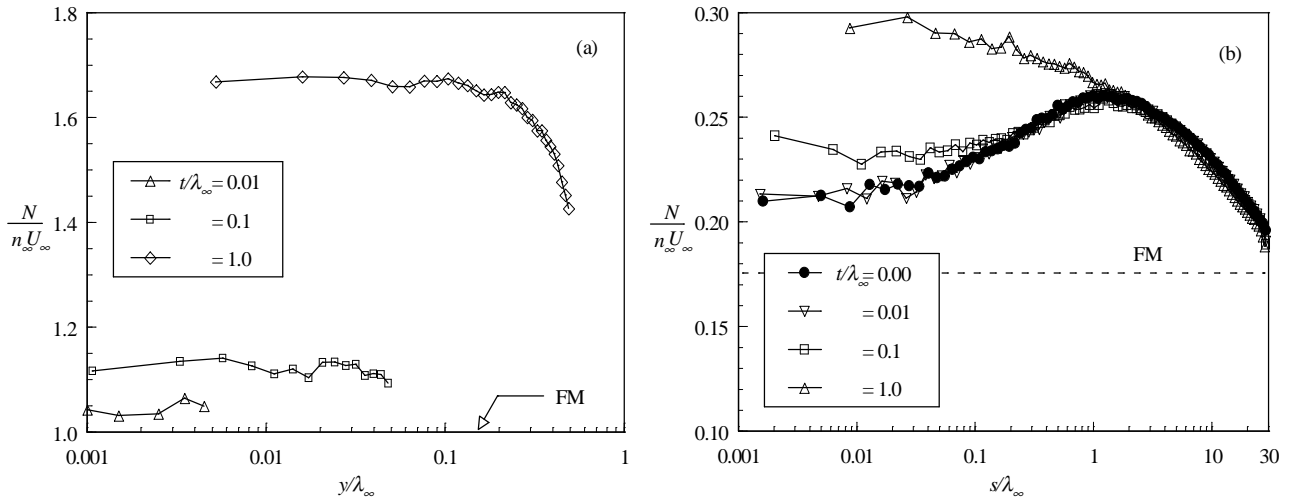

Figure 6: Dimensionless number flux along the (a) frontal face and (b) along the wedge surface as a function of the leading edge thickness.

The pressure p_w on the wedge surface is calculated by the sum of the normal momentum fluxes of both incident and reflected molecules at each time step. A flux is regarded as positive if it is directed toward the surface. Results are normalized by the freestream dynamic pressure $\frac{1}{2}\rho_\infty U_\infty^2$ and presented in terms of the pressure coefficient C_p.

The effects of the leading edge thickness on the pressure coefficient obtained by DSMC method are illustrated in Fig. (7). Figure (7a) shows the pressure coefficient on the frontal face as a function of the dimensionless height y/λ_∞ measured from the stagnation point to the shoulder of the wedge, and Fig. (7b) illustrates the pressure coefficient along the wedge surface as a function of the dimensionless arc length s/λ_∞ measured from the shoulder of the leading edge.

Referring to Fig. (7a), it can be seen that the pressure coefficient is basically constant along the frontal face, and increases the constant value with increasing Knudsen number Kn_t. As the number of molecules impinging on the frontal face decreases in the vicinity of the shoulder (see Fig. (6a)), then the normal component of the thermal velocity of the molecules increases as the flow approaches the shoulder of the leading edge.

The general shape of the pressure coefficient along the inclined surface is similar to that presented by the number flux, i.e., the pressure coefficient increases in the vicinity of the shoulder with falling Knudsen number Kn_t.

Plotted along with the computational solutions for pressure coefficient is the pressure coefficient predicted by the free molecular flow. As a reference, the free molecular flow values for pressure coefficient on frontal face and along the wedge surface are 2.35 and 0.12, respectively. Therefore, for the thinnest blunt leading edge ($t/\lambda_\infty = 0.01$) investigated, the flow seems to approach the free collision flow in the vicinity of the stagnation point (Fig. (7a)), as was

pointed out earlier. Nevertheless, according to Fig. (7b), the flow is far from free collision for the leading edge thicknesses investigated, even though for the sharp wedge (no thickness) case.
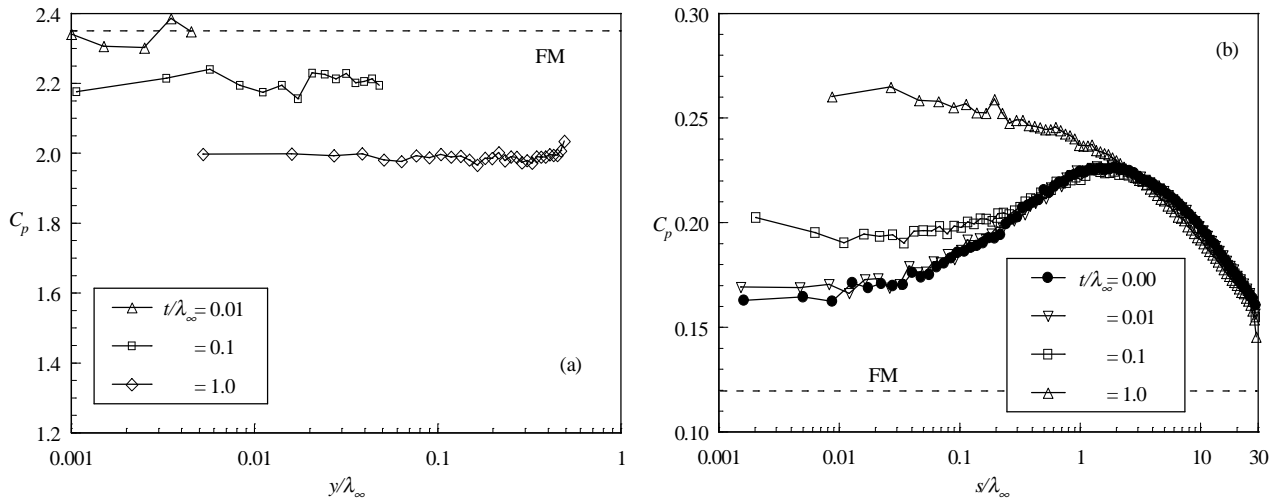

Figure 7: Pressure coefficient along the (a) frontal face and (b) along the wedge surface as a function of the leading edge thickness.

The heat flux q_w to the wedge surface is calculated by the net energy fluxes of the molecules impinging on the surface. The net heat flux is related to the sum of the translational, rotational and vibrational energies of both incident and reflected molecules. The heat flux is normalized by $\frac{1}{2}\rho_\infty U_\infty^3$, which corresponds to 2 MW/m^2 for the freestream conditions, and presented in terms of heat transfer coefficient C_h.

The heat flux was based upon the gas-surface interaction model of fully accommodated, completely diffuse re-emission. This is the most common model assumed, even though it is well known that some degree of specular re-emission and less than complete accommodation are more realistic assumptions. Furthermore, care should be taken in choosing the thermal accommodation coefficient for different altitude ranges, since the value of a thermal accommodation coefficient has a significant impact on the predicted aerodynamic heating, as pointed out by Gilmore and Harvey (1994).

The leading edge thickness effect on heat transfer coefficient is plotted in Figs. (8a) and (8b), which correspond to the frontal and inclined surfaces of the wedge, respectively. For purpose of comparison, the heat transfer coefficient predicted by the free molecular flow is also shown in both plots. It is seen from Fig. (8a) that the heat transfer coefficient is sensitive to the leading edge thickness. As would be expected, the blunter the leading edge is the lower the heat transfer coefficient along the frontal face. For the bluntest case investigated, $t/\lambda_\infty = 1.0$, the heat transfer coefficient increases in the vicinity of the shoulder. Based on the previous behavior for pressure coefficient, this behavior would be expected since the thermal velocity of the molecules increases in the vicinity of the shoulder on the frontal face. The contribution of the translational energy to the net heat flux varies with the square of the thermal velocity of the molecules.
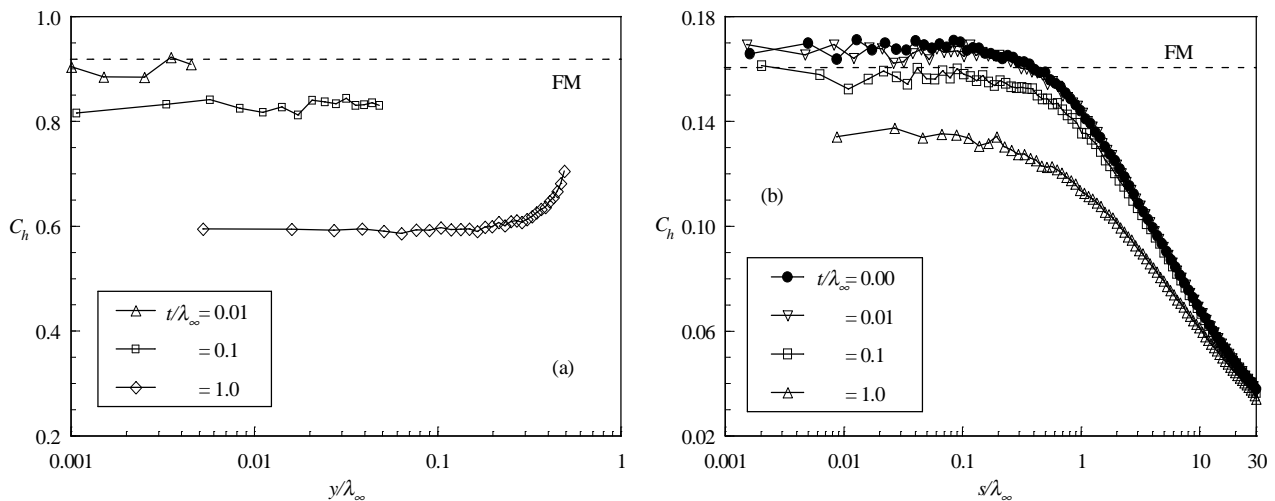

Figure 8: Heat transfer coefficient along the (a) frontal face and (b) along the wedge surface as a function of the leading edge thickness.

According to Fig. (8b), the effect of blunting the leading edge is to decreases the heat transfer coefficient on the inclined surface in the region near the shoulder of the wedges, as compared to the sharp wedge case.

The heat flux to the body surface was defined in terms of the incident and reflected flow properties. In order to better visualize the behavior of the heat transfer coefficient on the wedge surface, the incident C_{hi} and reflected C_{hr} contributions to the heat transfer coefficient C_h are illustrated in Figs. (9a) and (9b), respectively. According to these Figs., it is observed that the incident and reflected contributions present different behaviors. The difference is associated to the gas-surface interaction. The diffuse model assumes that the molecules are reflected equally in all directions, quite independently of their incident speed and direction. Due to the diffuse reflection model, the reflected thermal velocity of the molecules impinging on the surface is obtained from a Maxwellian distribution that takes into account for the temperature of the body surface. In this fashion, as the wall temperature is the same for all the cases investigated, the number of molecules impinging on the surface plays the important role on the reflected contribution to the net heat flux to the body surface.
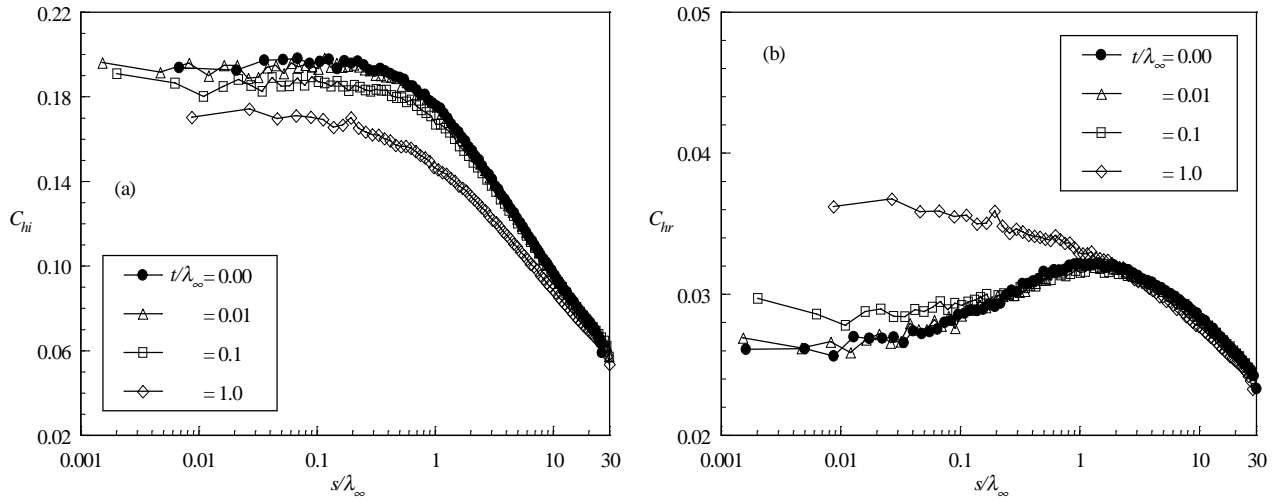

Figure 9: (a) Incident heat transfer coefficient and (b) reflected heat transfer coefficient along the wedge surface as a function of the leading edge thickness.

The shear stress τ_w on the body surface is calculated by averaging the tangential momentum transfer of the molecules impinging on the surface. For the diffuse reflection model imposed for the gas-surface interaction, reflected molecules have a tangential moment equal to zero, since the molecules essentially lose, on average, their tangential velocity component.

Results are normalized by $\frac{1}{2}\rho_\infty U_\infty^2$ and presented in terms of the dimensionless skin friction coefficient C_f. The influence of the leading edge thickness on the skin friction coefficient obtained by DSMC method are displayed in Fig. (10), parameterized by the dimensionless leading edge thickness. Figure (10a) illustrates the skin friction coefficient on the frontal face and Fig. (10b) depicts the skin friction coefficient along the wedge surface.
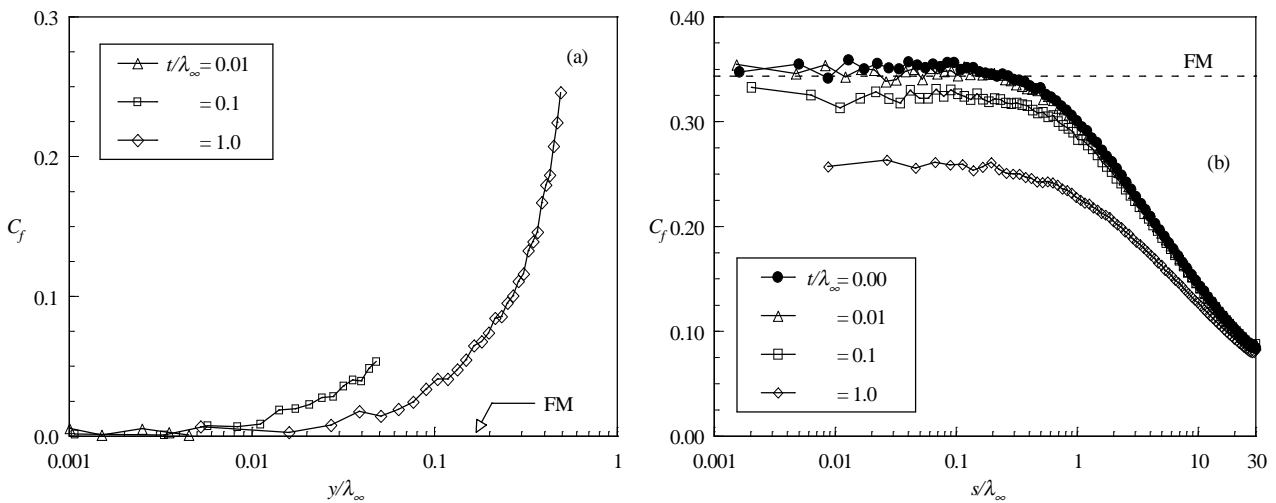

Figure 10: Skin friction coefficient along the (a) frontal face and (b) along the wedge surface as a function of the leading edge thickness.

According to Fig. (10a), the skin friction coefficient is zero at the stagnation point and increases along the frontal face up to the shoulder of the wedge. It means that the tangent momentum of the molecules is increasing due to the velocity of the molecules, since the number of molecules impinging on the frontal face decreases in the vicinity of the shoulder, as shown in Fig. (6a).

The general shape of the skin friction coefficient on the wedge surface is similar to that for the heat flux. Another interesting feature in the skin friction coefficient is that it is the same order of magnitude on both surfaces, in contrast to the pressure and heat transfer coefficients.

The drag on a surface in a gas flow results from the interchange of momentum between the surface and the molecules colliding with the surface. The total drag is obtained by the integration of the pressure p_w and shear stress τ_w distributions from the stagnation point of the leading edge to the station L that corresponds to the tangent point common to all the wedges (see Fig. (1)). It is worthwhile to mention that the values for the total drag were obtained by assuming the shapes acting as leading edges. Therefore, no base pressure effects were taken into account on the calculations. The DSMC results for total drag are normalized by $\frac{1}{2}\rho_\infty U_\infty^2 H$ and presented as total drag coefficient C_d and its components of pressure drag coefficient and the skin friction drag coefficient.

The extent of the changes in the drag coefficient C_d with increasing the leading edge thickness is demonstrated in Fig. (11). It is seen that as the leading edge becomes blunt the contribution of the pressure drag to the total drag increases and the contribution of the skin friction drag decreases. As the net effect on total drag coefficient depends on these to opposite behaviors, hence no appreciable changes are observed in the total drag coefficient for the leading edge thicknesses investigated.
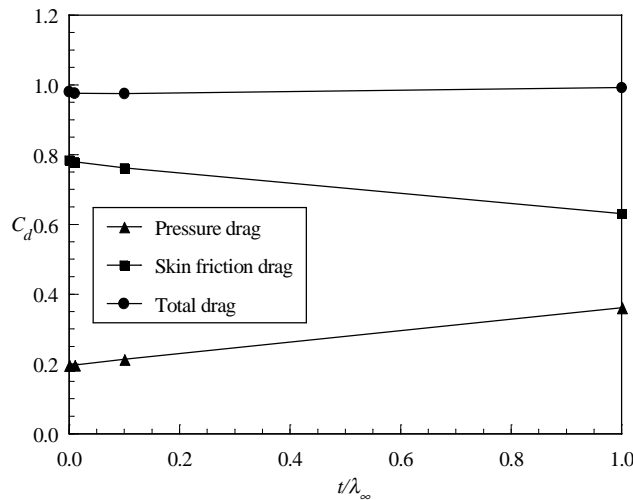

Figure 11: Pressure drag, skin friction drag and total drag coefficients as a function of the leading edge thickness.

4. Concluding Remarks

Through the use of DSMC method, the flow structure and the aerodynamic surface quantities about sharp/blunt wedges have been investigated. The calculations provided information concerning the nature of the flow at the vicinity of the nose resulting from variations in the leading edge thickness for the idealized situation of two-dimensional hypersonic rarefied flow.

Performance results for leading edge thicknesses (t/λ_∞) of 0.01, 0.1 and 1.0, indicated that the flow approaches the free molecular flow in the vicinity of the frontal face of the wedge as the leading edge thickness decreases, for the flow conditions considered. It was observed that even though for a slightly blunt leading edge, thickness of one hundredth of the freestream mean free path, the flow structure was affected far from the nose of the leading edge, when compared to the freestream mean free path.

Substantial changes in the surface quantities were observed as the leading edge thickness increased. Number flux and pressure coefficient increased in a region the order of the thickness downstream of the shoulder of the wedges. On the other hand, the heat transfer coefficient and the skin friction coefficient decreased and affected a larger region downstream the shoulder.

Results indicated that, with the size of the models being tested in hypersonic tunnels, large effects on flow structure and surface quantities due to leading edge thickness are possible even with models whose leading edges are generally considered as being aerodynamically sharp.

5. Acknowledgement

Institute for Space Research for use of the workstations.

6. References

Allègre, J., Herpe, G. and Faulmann, D., 1969, "Measurements of Pressure Distribution, Drag and Lift on Flat Plates and Wedges at Mach 8 in Rarefied Gas Flow", Proceedings of the 6th International Symposium on Rarefied Gas Dynamics, Vol. I, Ed. L. Trilling and H. Y. Wachman, Academic Press, New York, pp. 465-482.

Bertin, J. J., 1994, "Hypersonic Aerothermodynamics", AIAA Education Series, Washington D.C..

Bird, G. A., 1988, "Monte Carlo Simulation in an Engineering Context", Progress in Astronautics and Aeronautics: Rarefied gas Dynamics, Ed. Sam S. Fisher, Vol. 74, part I, AIAA New York, pp. 239-255.

Bird, G. A., 1994, "Molecular Gas Dynamics and the Direct Simulation of Gas Flows", Oxford University Press, Oxford, England, UK.

Borgnakke, C. and Larsen, P. S., 1975, "Statistical Collision Model for Monte Carlo Simulation of Polyatomic Gas Mixture", Journal of computational Physics, Vol. 18, pp. 405-420.

Cheng, H. K., Hall, J. G., Golian, T. C. and Hertzberg, A., 1961, "Boundary-Layer Displacement and Leading-Edge Bluntness Effects in High-Temperature Hypersonic Flow", J. of the Aerospace Sciences, Vol. 28(5), pp. 353-381.

Gilmore, M. R. and Harvey, J. H., 1994, "Effects of Mach Number, T_{wall}, T_∞ and Thermal Accommodation Coefficient on Flow Around Bluff Bodies in Rarefied Regime", Rarefied Gas Dynamics: Space Science and Engineering, edited by B. D. Shizgal and D. P. Weaver, Vol. 160, Progress in Astronautics and Aeronautics, AIAA New York, pp. 308-322.

Gupta, R. N., Scott, C. D., and Moss, J. N., 1985, "Slip-Boundary Equations for Multicomponent Nonequilibrium Airflow", NASA TP-2452.

Haas, B. L., Fallavollita, M. A., 1994, "Flow Resolution and Domain Influence in Rarefied Hypersonic Blunt-Body Flows", Journal of Thermophysics and Heat Transfer, Vol. 8(4), pp. 751-757.

Klemm, F. J. and Giddens, D. P., 1977, "A Numerical Solution to the Problem of Low-Density Hypersonic Wedge Flow", Rarefied Gas Dynamics, Progess in Astronautics and Aeronautics, vol. 51, Part I, Ed. J. L. Potter, pp. 313-322.

Liepmann, H. W., Narasimha, R. and Chahine, M., 1964, "Theoretical and Experimental Aspects of the Shock Structure Problem", Proceedings of the 11th International Congress of Applied Mechanics, Ed. H. Gortler, Munich, Germany, pp. 973-979.

McCroskey, W. J., Bogdonoff, S. M. and Genchi, A. P., 1967, "Leading Edge Flow Studies of Sharp Bodies in Rarefied Hypersonic Flow", Proceedings of 5th International Symposium on Rarefied Gas Dynamics, Vol. II, Ed. C. L. Brundin, Academic Press, New York, pp. 1047-1066.

Tincher, D. and Burnett, D., 1994, "A Hypersonic Waverider Flight Test Vehicle: The Logical Next Step", J. of Spacecraft and Rockets, Vol. 31(3), pp.392-399.

Vidal, R. J. and Bartz, J. A., 1965, "Experimental Studies of Low-Density Effects in Hypersonic Wedge Flows", Proceedings of the 4th International Symposium on Rarefied Gas Dynamics, vol. 1, Ed. J. H. de Leeuw, Academic Press, New York, pp. 467-486.

Vidal, R. J. and Bartz, J. A., 1969, "Surface Measurements on Sharp Flat Plates and Wedges in Low-Density Hypersonic Flow", AIAA Journal, Vol. 7(6), pp. 1099-1109.